Letters

Low-Cost Realization of Feature Position Estimation Scheme for Switched Reluctance Motor

Rajdeep Banerjee, *Student Member, IEEE*, and Parthasarathi Sensarma, *Senior Member, IEEE*

***Abstract*—This letter proposes a low-cost feature position estimation scheme for singly excited SRM without using lookup tables. This scheme uses the particular flux linkage versus current curve, corresponding to the commutation angle, to generate a flux-linkage reference. Phase commutation is executed at the instant when the online estimated flux linkage reaches this reference threshold. So, this letter, initially, proposes a novel analytical method to compute the reference flux linkage from phase currents. Then, a new approach is presented that maps the individual measured phase currents and estimated flux linkages into corresponding unified signals to reduce the computational burden. Thereafter, the mutual coupling among phases is shown as a cause of serious error in the thresholding operation, and a design criterion to avoid this error is derived. Performance of the proposed sensorless scheme is experimentally validated on a 1 kW, 3000 r/min, 6/4 SRM-based laboratory prototype.**

***Index Terms*—Flux-linkage characteristics, nonlinear model, sensor-less, SRM.**

NOMENCLATURE

ABC	Asymmetric bridge converter.
ACW, CW	Anticlockwise, clockwise.
ADC	Analog to digital converter.
AND	Logical "AND" operation.
FPGA	Field programmable gate array.
FSM	Finite state machine.
IGBT	Insulated gate bipolar transistor.
LUT	Lookup table.
MUX	Multiplexer.
SD	Standard deviation.
SRM	Switched reluctance motor.

I. INTRODUCTION

THE feature position estimation scheme is widely used for switched reluctance motor drives in medium and high-speed applications [1], [2], [3], [4]. This scheme, initially, synthesizes a flux-linkage reference, ψ_{ref}, from the excitation current, i, using the flux-linkage characteristic, $\psi(i, \theta_{\text{off}})$, for the commutation angle, θ_{off}. Then, the excited phase is commutated at the instant when the corresponding estimated flux linkage, $\hat{\psi}$, equals ψ_{ref}, and the next phase, in sequence, is excited. This ensures that the dwell angle is equal to the stroke angle σ. A design tradeoff exists between the requirement of data memory and processing speed for realizing this scheme on a digital platform. In [2], ψ_{ref} in terms of all the phase currents are stored in an LUT that requires significantly large data space. However, in [3] and [4], the Fourier series-based analytical model is proposed, which represents ψ_{ref} as a function of rotor position θ. These Fourier coefficients are defined as higher degree (>2) polynomials in i. Computation of these polynomials increases the number of mathematical operations that leads to requirement of a high machine clock frequency for the digital controller. Either one of the aforementioned cases increases the cost of digital controller.

Therefore, this letter reports a twofold solution. First, to eliminate the use of LUTs, a novel analytical model for $\psi(i, \theta)$ is presented that represents the flux linkage ψ as a function of i for each rotor position θ. The proposed model considers the effect of "S"-shaped magnetic nonlinearity (B-H curve) on $\psi(i, \theta_{\text{off}})$. Second, to minimize the mathematical operations, an algorithm is proposed that computes the unified signals of $\hat{\psi}$ and ψ_{ref} instead of computing these for each phase individually. Then, considering the effect of mutual inductance, the drive signals are synthesized sequentially using an FSM. Finally, experimental results are presented for validation.

II. SRM DRIVES CONFIGURATION

Fig. 1(a) shows the schematic diagram for an SRM-based variable speed drive, comprising a 6/4 SRM and asymmetric bridge converter. Each phase of the power converter comprises two switches $\{Q_{n1}, Q_{n2}\}$ and two diodes $\{D_{n1}, D_{n2}\}$. The drive signal X_n for Q_{n2} decides the excitation region of nth phase with respect to corresponding rotor position θ_n. Here, θ_n is defined with respect to the unaligned position of nth phase. The drive signal pwm_n for Q_{n1} is generated, while corresponding $X_n = 1$, to control the phase current i_n. Therefore, the effective voltage v_n across the nth excited phase is expressed as [1]

$$v_n = d(t)V_{\text{dc}} = Ri_n + \frac{d\psi_n}{dt}, \quad n \in \{1, 2, 3\} \tag{1}$$

Manuscript received 7 September 2022; revised 21 October 2022; accepted 11 November 2022. Date of publication 16 November 2022; date of current version 26 December 2022. *(Corresponding author: Rajdeep Banerjee.)*

The authors are with the Department of Electrical Engineering, Indian Institute of Technology Kanpur, Kanpur 208016, India (e-mail: brajdeep@iitk.ac.in; sensarma@iitk.ac.in).

Color versions of one or more figures in this article are available at https://doi.org/10.1109/TPEL.2022.3222739.

Digital Object Identifier 10.1109/TPEL.2022.3222739

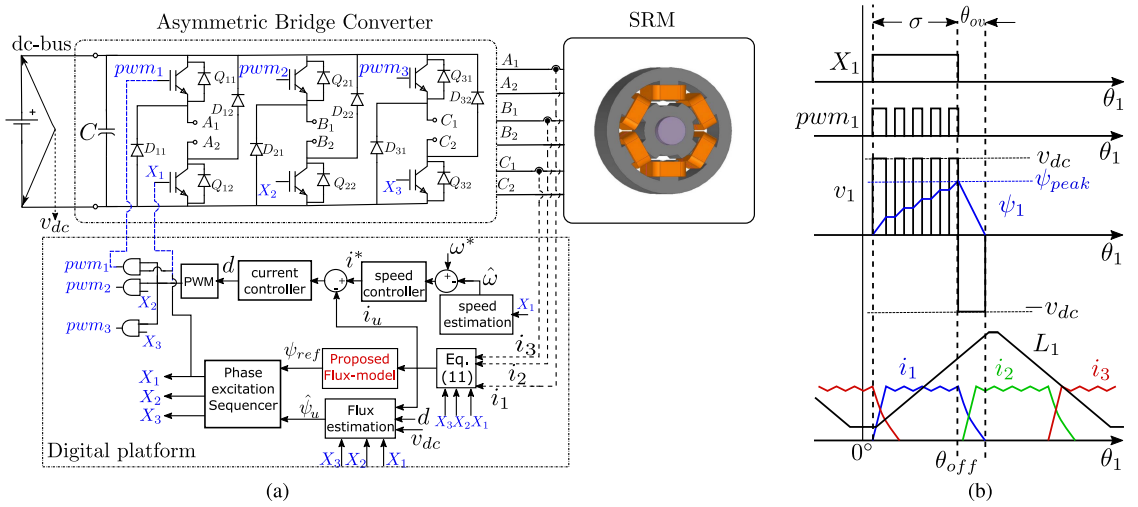

Fig. 1. (a) Schematic diagram for a 6/4 SRM drive along with sensorless control scheme. (b) Typical waveforms of X_n, pwm_n, v_n, i_n, and ψ_n.

where V_{dc} and $d(t)$ denote the dc-link voltage and duty ratio of corresponding pwm_n, respectively. ψ_n and R are the developed flux linkage and winding resistance of nth phase, respectively. At steady state, Fig. 1(b) shows the typical waveforms of v_n, i_n, and ψ_n with respect to θ_1. At the turn-OFF instant, $\theta_1 = \theta_{\text{off}}$, ψ_n reaches its maximum value ψ_{peak}. Neglecting (Ri_n) drop in (1), ψ_{peak} is expressed in terms of v_n at a particular rotor speed ω so that

$$\psi_{\text{peak}} = \frac{1}{\omega}\int_{\theta_{\text{off}}-\sigma}^{\theta_{\text{off}}} v_n d\theta = \frac{V_{\text{dc}}}{\omega}\int_{\theta_{\text{off}}-\sigma}^{\theta_{\text{off}}} d(t)d\theta. \tag{2}$$

Simplifying further, using the mean duty ratio D

$$\psi_{\text{peak}} = \frac{DV_{\text{dc}}\sigma}{\omega}, \text{where } D = \frac{1}{\sigma}\int_{\theta_{\text{off}}-\sigma}^{\theta_{\text{off}}} d(t)d\theta_n. \tag{3}$$

Both the switches are turned-OFF at $\theta_1 = \theta_{\text{off}}$, which forces i_n to flow through the diodes. That phase enters the deenergizing zone during which i_n decays to zero, since $v_n{=}{-}V_{\text{dc}}$. Angular duration θ_{ov} of this deenergizing zone is expressed as

$$\theta_{\text{ov}} = \frac{\psi_{\text{peak}}\omega}{V_{\text{dc}}}. \tag{4}$$

To control the SRM drive, in general, a two-loop hierarchical control scheme, comprising inner current and outer speed loops, is considered. Here, d is computed by the current controller so that i_n tracks the reference current i^*. The speed controller generates i^* to maintain a desired rotor speed ω^*. An estimate of rotor speed $\hat{\omega}$ is used for feedback, and is computed from an arbitrarily chosen drive signal X_n [8] as

$$\hat{\omega}(\text{in r/min}) = \frac{60}{N_r \Delta T} \tag{5}$$

where N_r is the rotor pole number and ΔT the period of X_n. A free-running clock, with period T_{clk}, increments a digital counter over the time period of X_n and the final count corresponds to ΔT. The bit size Γ of the counter register defines the minimum

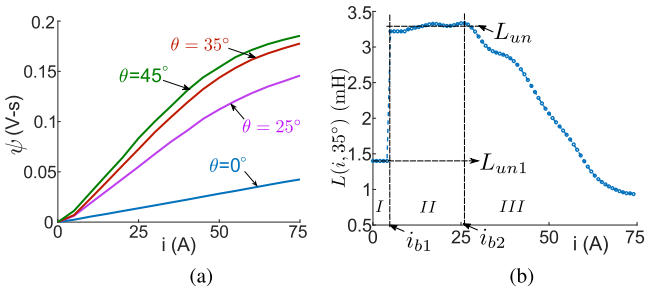

Fig. 2. (a) Flux-linkage characteristics obtained experimentally for a 6/4 SRM, (b) variation of L with i at 35° (mech.).

speed ω_{cr} that can be correctly estimated

$$\omega_{\text{cr}}(\text{in r/min}) = \frac{60}{2^{\Gamma}T_{clk}N_r}. \tag{6}$$

Drive signals $X_n(n \in \{1,2,3\})$ are synthesized from the position sensorless scheme, discussed as follows.

III. Proposed Sensorless Scheme

In the proposed feature sensorless scheme, the reference flux linkage $\psi(i,\theta_{\text{off}})$, corresponding to predecided θ_{off}, is computed using a novel online method discussed as follows.

A. Proposed Flux-Linkage Reference Computation

Fig. 2(a) shows the experimentally obtained $\psi(i,\theta)$ for a 6/4 SRM. Here, $\theta = 0°$ and $45°$ (mech.) denote the unaligned and aligned rotor positions, respectively. For motoring, phase excitation interval is enclosed by these limits. To validate the proposed scheme, $\theta = 35°$ (mech.) is chosen arbitrarily as θ_{off}, which ensures the excitation of each phase in the positive gradient region of corresponding phase inductance. Hence, from $\psi(i,35°)$, the phase inductance $L(i,35°)$, corresponding to $\theta =$

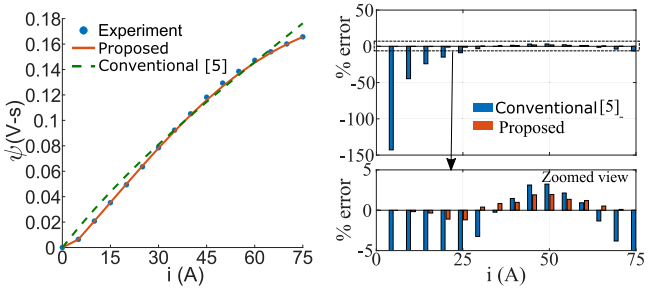

Fig. 3. (a) Comparison of $\psi - i$ curves, computed using proposed and existing computation methods [5], with experimental data and (b) error analysis for both the methods.

35° (mech.), is computed using

$$L(i, 35^\circ) = \frac{\psi(i, 35^\circ)}{i} \tag{7}$$

and is shown in Fig. 2(b). It is observed that it has three different regions based on i. Here, i_{b1} and i_{b2} denote the boundary currents between these regions, defined as follows,

1) *Region-I* $\{0 \le i \le i_{b1}\}$: $L(i, \theta) = L_{\text{un1}}$ which is less than the unsaturated inductance L_{un} due to initial nonlinearity of *B-H* curve.
2) *Region-II* $\{i_{b1} < i \le i_{b2}\}$: $L(i, \theta)$ remains constant and equal to the unsaturated inductance L_{un}.
3) *Region-III* $\{i > i_{b2}\}$: $L(i, \theta)$ is decreases with i due to magnetic saturation.

In [5], $L(i, \theta)$ is approximated using the rational fraction considering the magnetic saturation only. Therefore, to incorporate $L(i, \theta)$ of region-I, the flux linkage $\psi_e(i, \theta)$ is computed from the measured current i for an arbitrary θ as follows

$$\psi_e(i, \theta) = \begin{cases} L_{\text{un1}} i, & i < i_{b1} \\ \frac{L_{\text{un}}(i - i_{b1})}{1 + a_0(i - i_{b1}) + a_1(i - i_{b1})^2} + L_{\text{un1}} i_{b1}, & i \ge i_{b1}. \end{cases} \tag{8}$$

Here, L_{un1} and L_{un} are the mean values of $L(i, 35^\circ)$ in region-I and region-II, respectively, whereas i_{b1} corresponds to the first point of discontinuity in $L(i, 35^\circ)$ near $i = 0$. Rearranging (8)

$$\frac{L_{\text{un}}(i - i_{b1})}{\psi - L_{\text{un1}} i_{b1}} = 1 + a_0(i - i_{b1}) + a_1(i - i_{b1})^2 \tag{9}$$

the coefficients a_0 and a_1 are obtained from a least squares fit over the entire data ψ_m of ψ, which is either measured or computed, for $i \ge i_{b1}$. Fig. 3(a) shows the comparison between flux-linkage characteristics, obtained from the experimental measurement, and computed using existing [5] and proposed online methods. Model errors are quantified as

$$\epsilon(i) = \frac{\psi_e(i, 35^\circ) - \psi_m(i, 35^\circ)}{\psi_e(i, 35^\circ)}. \tag{10}$$

Fig. 3(b) plots this error, as a percentage, and the improved accuracy of the proposed model is clearly observed. Now, the sequential generation of drive signals X_n using the proposed model is discussed as follows.

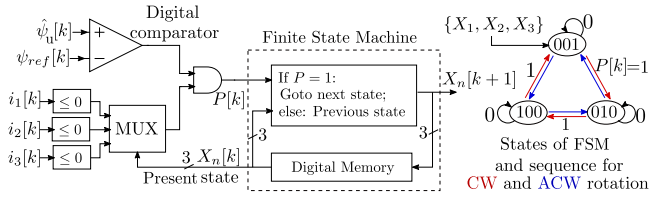

Fig. 4. Generation of $X_n (n \in \{1, 2, 3\})$ using an FSM and its state diagram.

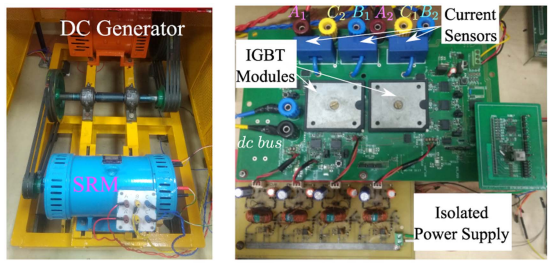

Fig. 5. Experimental setup. (a) SRM. (b) ABC with auxiliary circuits.

B. Generation of Drive Signals

Fig. 1(a) shows the schematic of the proposed sensorless control scheme. Since each phase is excited at a time

$$\sum_n X_n = 1, \quad n \in \{1, 2, 3\}. \tag{11}$$

This helps to define a unified flux linkage ψ_u as

$$\psi_u = \sum_n X_n \psi_n, \quad n \in \{1, 2, 3\}. \tag{12}$$

Also, phase currents i_n are sensed and mapped into a unified current signal i_u as follows:

$$i_u = \sum_n X_n i_n, \quad n \in \{1, 2, 3\} \tag{13}$$

which serves as the unique feedback signal for the current controller. Here, it is also used to compute the reference flux linkage $\psi_{\text{ref}}(\theta_{\text{off}})$ using (8), for the predecided θ_{off}. Computing an estimate $\hat{\psi}_n$ of ψ_n as

$$\hat{\psi}_n[k+1] = \begin{cases} (d[k] v_{\text{dc}}[k] - R i_u[k]) T_s + \hat{\psi}[k], & \text{for } X_n = 1 \\ 0, & \text{for } X_n = 0 \end{cases} \tag{14}$$

an estimate $\hat{\psi}_u$ of ψ_u, as per (12), is computed as follows:

$$\hat{\psi}_u[k+1] = \sum_n X_n \hat{\psi}_n[k+1] \tag{15}$$

where T_s denotes the sampling time.

Fig. 4 shows a schematic to synthesize X_n by comparing $\psi_{\text{ref}}(\theta_{\text{off}})$ and $\hat{\psi}_u$ at each sampling instant. Although each phase is excited at a time, there is an overlap region while i_n of consecutive phases are nonzero, as shown in Fig. 1(b). During this overlapped region, θ_{ov}, ψ_n corresponding to the excited phase is expressed as [2],

$$\psi_n = L_n i_n + M_{nq} i_q, n \ne q; \; n, q \in \{1, 2, 3\} \tag{16}$$

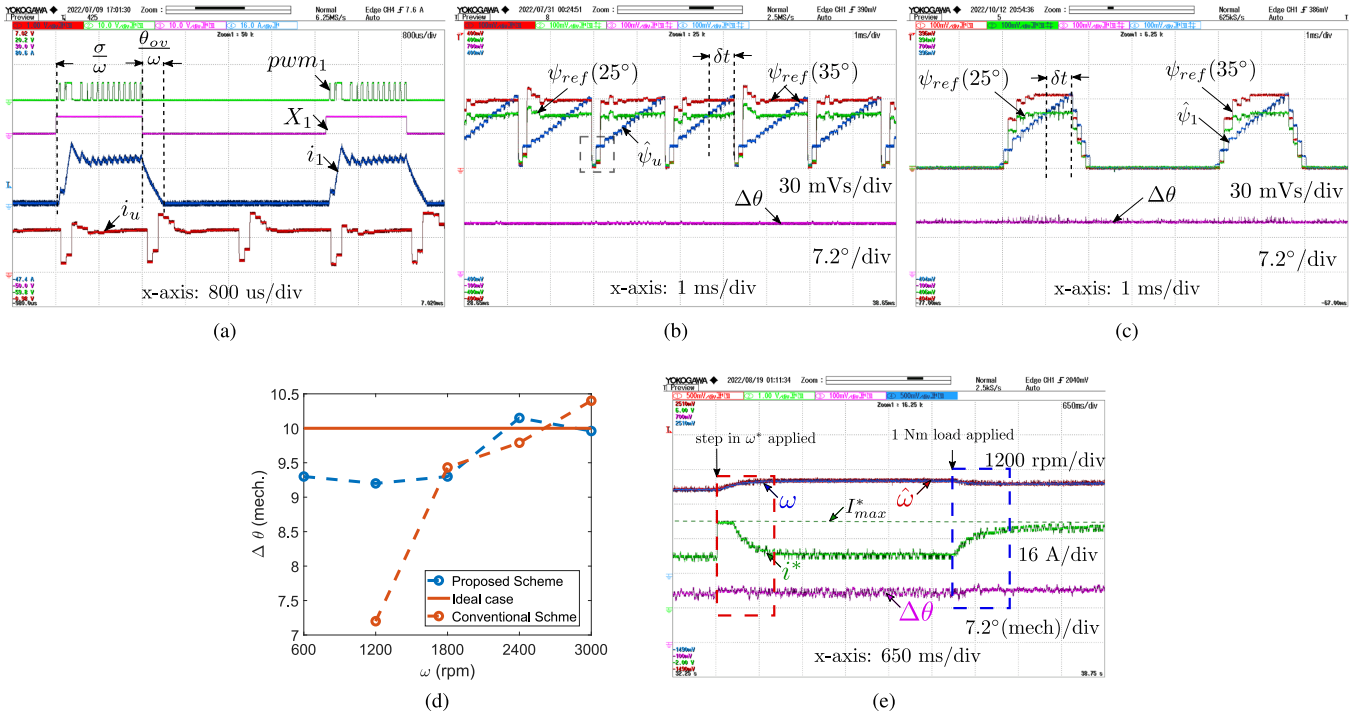

Fig. 6. Experimental results: (a) pwm_1, X_1, i_1, and i_u, while ω=3000 r/min; $\psi_{\mathrm{ref}}(25^\circ)$, $\psi_{\mathrm{ref}}(35^\circ)$, $\hat{\psi}_u$, and $\Delta\theta$ while ω=3000 r/min for (b) proposed and (c) conventional sensorless scheme [2], (d) $\Delta\theta$ at different operating ω, (e) ω, $\hat{\omega}$, i^*, and $\Delta\theta$ during step in ω^* and T_l. Scale: (a) i_1, i_u (16 A/div), time:800 μs/div; (b), (c) $\psi_{\mathrm{ref}}(25^\circ)$, $\psi_{\mathrm{ref}}(35^\circ)$, $\hat{\psi}$ (30 mVs/div), $\Delta\theta$ (7.2° mech./div), and time: 1 ms/div; (e) ω, ω^* (1200 r/min/div), i^* (16 A/div), $\Delta\theta$ (7.2°mech./div), time:650 ms/div.

where the suffixes n and q correspond to the present and previously excited phases, respectively, and M is their mutual inductance. Since the effect of M is not incorporated in the reference dataset ψ_m, mere comparison of $\hat{\psi}_u$ and $\psi_{\mathrm{ref}}(\theta_{\mathrm{off}})$ will not ensure accurate determination of θ_{off}. To eliminate this problem, this comparison is activated after $i_q \leq 0$, i.e., after the elapse of θ_{ov}. Therefore, to avail at least one sampling interval after the activation, it is clear that θ_{ov} must be less than σ. Substituting ψ_{peak} from (3) in (4)

$$\theta_{\mathrm{ov}} = D\sigma \tag{17}$$

a criterion formulated for a given ω and T_s is expressed as

$$\omega T_s \leq \sigma(1-D). \tag{18}$$

During running condition, $X_n(n \in 1,2,3)$ are generated from an FSM where its states are all possible combinations of X_n as per (11). Fig. 4 shows the state diagram for CW and ACW rotations of the rotor. State transition, leading to phase commutation, occurs when its binary input $P[k]$ is a logic "1." A MUX selects the binary result of signum comparison, $i_q \leq 0$, for the current i_q in the previously excited phase. The logical AND ensures that phase commutation happens when

$$P[k] = \{\hat{\psi}[k] \geq \psi_{\mathrm{ref}}(\theta_{\mathrm{off}})[k]\} \cap \{i_q \leq 0\} = 1. \tag{19}$$

At stand still, the initial state is decided either using initial position estimation schemes, [6], [7], [8], [9], or from position sensors. Experimental validation of the proposed scheme is presented in the following section.

TABLE I
OPERATING CONDITIONS FOR 6/4 SRM

dc-link voltage (V_{dc})	190 V
Rated speed	3000 r/min
Maximum current reference (I^*_{max})	40 A
Maximum load torque (T_l)	2.4 N·m
Sampling rate ($1/T_s$)	10 kHz

IV. EXPERIMENTAL VALIDATION

Fig. 5 shows the 1 kW, 3000 r/min, 6/4 SRM-based laboratory prototype along with asymmetric bridge converter (ABC) and its auxiliary circuits. Two three-phase IGBT-based inverter modules (Semkron Skiip28AC066V1) are used for the power circuit of the ABC. The detailed operating conditions are listed in Table I. The proposed sensorless scheme and the controllers are implemented on an FPGA (Altera Cyclone)-based digital platform, with 20 MHz clock frequency. Feedback variables V_{dc} and i_n are sampled at the switching frequency and digitized using an on-board ADC.

Fig. 6(a) shows the experimental result of the drive signals pwm_1 and X_1, i_1, and i_u while $\omega = 3000$ r/min. It is observed that peaks of i_1 are mapped into i_u while $X_1 = 1$ as per (13), and i_u is an uninterrupted signal.

Having arbitrarily chosen $\theta_{\mathrm{off}} = 35^\circ$, the reference flux linkage $\psi_{\mathrm{ref}}(35^\circ)$ is computed using (8) as per the proposed model. Also, a pseudoreference signal $\psi_{\mathrm{ref}}(25^\circ)$, for $\theta = 25^\circ$ (mech.), is computed to verify the proposed model. With a pair of Schimdt

triggers toggling at $\hat{\psi}_u = \psi_{\rm ref}(25^\circ)$ and $\hat{\psi}_u = \psi_{\rm ref}(35^\circ)$, the time interval δt between these two events is measured. The corresponding angle $\Delta\theta$ is expressed at the operating speed ω as

$$\Delta\theta = \omega\delta t. \tag{20}$$

In this case, $\Delta\theta$ should ideally be 10° (mech.). Fig. 6(b) shows the experimental result of $\hat{\psi}_u$, $\psi_{\rm ref}(35^\circ)$, $\psi_{\rm ref}(25^\circ)$, and $\Delta\theta$, respectively, while ω=3000 r/min. It is observed that $\Delta\theta$=9.936° (mech.). This ensures the accuracy of feature position $\theta_{\rm off}$=35° estimation using the proposed scheme. The effect of mutual coupling is observed near the turn-ON angle (enclosed by a dotted box), where both the reference signals $\psi_{\rm ref}(25^\circ)$ and $\psi_{\rm ref}(35^\circ)$ are less than $\hat{\psi}_u$. Spurious state transition in this region is avoided by disabling this comparison using (19). Performance of the proposed scheme is benchmarked against a conventional sensorless scheme [2], where two separate LUTs are used. These store the measured flux linkage versus current profiles for θ=25° and 35°, which are used to obtain $\psi_{\rm ref}(25^\circ)$ and $\psi_{\rm ref}(35^\circ)$, respectively, for each phase current i_n. Also, an estimate, $\hat{\psi}_n$ of ψ_n, for each phase is computed at the kth sampling instant using

$$\hat{\psi}_n[k+1] = (d[k]V_{\rm dc}[k] - Ri_n[k])\,T_s + \hat{\psi}_n[k], n \in \{1,2,3\}. \tag{21}$$

Fig. 6(a) shows the experimental results of $\hat{\psi}_1$, $\psi_{\rm ref}(35^\circ)$, and $\psi_{\rm ref}(25^\circ)$, at ω=3000 r/min, for the conventional method [2] where it is observed that $\Delta\theta$=10.4°(mech.). So the error is marginally more than that with the reported scheme.

To check the accuracy, Fig. 6(d) plots the measured $\Delta\theta$ at different operating speeds for both proposed and conventional schemes. Mean and SD of errors in measured $\Delta\theta$ are 0.42° (4.2%) and 0.43° (4.3%), respectively, for the proposed scheme, whereas for the conventional scheme, these are 0.79° (7.9%) and 1.39°, (13.9%), respectively. This confirms that accuracy of the proposed scheme is independent of ω. Robustness of the proposed scheme is examined under steps in speed reference ω^* and load torque T_l, which cause time varying i^* during transients. Fig. 6(e) shows the experimental result of estimated ($\hat{\omega}$) and actual (ω) speeds, reference current, i^* and $\Delta\theta$ for successive steps in command, ω^* (3000 to 3300 r/min), and disturbance, T_l (1 N · m). Estimated speed $\hat{\omega}$ is seen to accurately track the actual speed ω. Mean of $\Delta\theta$ is 10.6° during the speed transient, shown in the red box, whereas it is 10.8° (mech.) during the load transient, shown enclosed in the blue box.

V. Conclusion

This letter presented a low-cost realization of feature position estimation scheme for the SRM drive. The requirement of huge data memory is eliminated by using a novel online approach for flux-linkage reference computation, using measured phase currents. Then, the computation time is minimized by proposing an algorithm that computes the unified reference and estimated flux linkages, instead of computing for each phase. Also, a design criterion was derived to eliminate the effect of mutual coupling. This proposed scheme was experimentally validated on a 6/4 SRM drive and benchmarked against a conventional scheme. Estimation errors were less than 8% for different operating speeds as well as for the speed and load transients. However, the proposed scheme would still require conventional initial position estimation schemes for initial rotor position detection at start-up.

Acknowledgment

The authors would like to acknowledge Mr Amit Kr. Basu and Mr. Nandkishore for their support in development of the laboratory prototype.

References

[1] D. Xiao, S. R. Filho, G. Fang, J. Ye, and A. Emadi, "Position-sensorless control of switched reluctance motor drives: A review," *IEEE Trans. Transp. Electrif.*, vol. 8, no. 1, pp. 1209–1227, Mar. 2022, doi: 10.1109/TTE.2021.3110867.

[2] J. P. Lyons, S. R. MacMinn, and M. A. Preston, "Flux-current methods for SRM rotor position estimation," in *Proc. Conf. Rec. IEEE Ind. Appl. Soc. Annu. Meeting*, 1991, pp. 482–487, doi: 10.1109/IAS.1991.178199.

[3] T. Wang, W. Ding, Y. Hu, S. Yang, and S. Li, "Sensorless control of switched reluctance motor drive using an improved simplified flux linkage model method," in *Proc. IEEE Appl. Power Electron. Conf. Expo.*, 2018, pp. 2992–2998, doi: 10.1109/APEC.2018.8341445.

[4] W. Ding and K. Song, "Position sensorless control of switched reluctance motors using reference and virtual flux linkage with one-phase current sensor in medium and high speed," *IEEE Trans. Ind. Electron.*, vol. 67, no. 4, pp. 2595–2606, Apr. 2020, doi: 10.1109/TIE.2019.2912764.

[5] R. Banerjee and P. Sensarma, "Non-linear magnetic characteristics modeling for switched reluctance machines," in *Proc. IEEE Int. Conf. Power Electron., Drives Energy Syst.*, 2018, pp. 1–6, doi: 10.1109/PEDES.2018.8707800.

[6] J. Cai and Z. Deng, "Initial rotor position estimation and sensorless control of SRM based on coordinate transformation," *IEEE Trans. Instrum. Meas.*, vol. 64, no. 4, pp. 1004–1018, Apr. 2015, doi: 10.1109/TIM.2014.2364699.

[7] H. Gao, F. R. Salmasi, and M. Ehsani, "Sensorless control of SRM at standstill," in *Proc. 16th Annu. IEEE Appl. Power Electron. Conf. Expo.*, 2001, pp. 850–856, doi: 10.1109/APEC.2001.912468.

[8] R. Banerjee and P. Sensarma, "On-line detection and mitigation of faulty position-signal for switched reluctance motors," in *Proc. IEEE Int. Conf. Power Electron., Drives, Energy Syst.*, 2020, pp. 1–6, doi: 10.1109/PEDES49360.2020.9379611.

[9] J. Bu and L. Xu, "Eliminating starting hesitation for reliable sensorless control of switched reluctance motors," *IEEE Trans. Ind. Appl.*, vol. 37, no. 1, pp. 59–66, Jan./Feb. 2001, doi: 10.1109/28.903127.